UV-converted heterogeneous wettability surface for the realization of printed micro-scale conductive circuits

Ke Shui,[1,2,3] Yuxiao Fang,[2] Zerui Li,[2,3] Zhenguo Wang,[2,3] Subin Jiang,[4] Ni Yin,[3] Qi Chen,[3] Feng-Qi Guo,[1,*] Jian-Wen Zhao,[2] Jian Lin,[2,3,4] Chang-Qi Ma[2,3,4,*]

[1] School of Henan Institute of Advanced Technology, Zhengzhou University, 97 Wenhua Road, Zhengzhou, 450000 P. R. China

[2] Printable Electronics Research Center, Suzhou Institute of Nano-Tech and Nano-Bionics, Chinese Academy of Sciences, SEID, SIP, 215123, Suzhou, P. R. China

[3] *i-Lab*, Suzhou Institute of Nano-Tech and Nano-Bionics, Chinese Academy of Sciences, SEID, SIP, 215123, Suzhou, P. R. China

[4] Engineering Center of Precision Printing Manufacturing, Guangdong Institute of Semiconductor Micro-Nano Manufacturing Technology, Kejiao Road No. 1, Shishan Town, 528225 Foshan, P. R. China

Email: fqguo@zzu.edu.cn (FQGuo) cqma2011@sinano.ac.cn (CQMa)

Abstract:

Achieving high precision in the fabrication of electronic circuits through additive manufacturing requires breaking the resolution limit of traditional printing processes. To address this challenge, we have developed a novel approach that involves preparing a heterogeneous wetting surface using a light-sensitive NBE-acrylate resin. By creating differences in surface energy on the substrate, we can limit the spread of the ink and surpass the limitations of conventional processes, achieving a printing resolution of 5 μm. The NBE-acrylate resin can be cross-linked under white LED light illumination (with $\lambda > 400$ nm) to yield a hydrophobic surface, which can be converted to a hydrophilic surface by UV light illumination ($\lambda = 254$ nm). The photochemical reaction of the NBE-acrylate resin under different light irradiation was confirmed by FTIR and AFM microforce measurements. In combination with a photomask, patterned heterogeneous wettability surfaces were prepared, which can be utilized for printing precision electronic circuits. Micrometer-scale printed circuits with a low line-to-space (L/S) of 5/50 and 10/10 μm were successfully achieved by optimizing the ink formulation, which is significantly beyond the printing resolution. In the end, fully printed thin film transistor arrays based on semi-conducting carbon nanotubes were achieved, which showed higher charge carrier mobilities of 1.89-4.31 $cm^2 s^{-1} V^{-1}$ depending on the channel width, demonstrating the application of this precision printed technique.

Introduction

Printed electronics is a new technology that uses traditional printing (or coating) to manufacture electronic components and products.[1] It has a broad development prospect for its advantages, such as material saving,[2] environments friendly,[3] low-cost,[4] and most importantly, the flexible substrate and large-area production compatibility.[5-7] Compared to conventional subtractive lithography, the printing process showed poorer precision and lower lateral resolution, limiting the line-to-space to tens of micrometers.[8-11]. This has become the biggest obstacle to the large-scale application of printed electronics technology. Increasing the printing resolution is of great interest in modern electronic precision fabrication.[12] Among various methods, a combination of surface energy confinement effect and printing process that utilizes a pre-patterned hydrophilic-hydrophobic surface is considered a promising method and has attracted much research attention in the last few years.[13-15]

Limiting the diffusion of ink on the surface is crucial for reducing the pattern size. On the patterned wettability surface with heterogeneous surface energy in different regions, the motion of droplets depends on the gradient of surface energy.[16] Creating a patterned chemical/physical structure with different surface energy on the substrate are effective methods to control the wetting behavior of ink droplets on the substrate, reduce the diffusion of ink solution, and improve the printing resolution.[17] Wettability gradient can make ink droplets self-aligned during printing, which is a method of preparing ultra-fine structures. For example, Kooij[18] *et al*. used a self-assembled fluoroalkylsilane monolayer to deposit hydrophobic lines on the hydrophilic SiO_2 surface and successfully guided the movement of droplets by controlling the space between lines.

Researchers have discovered different ways to control the surface energy of insect-repellent porous polyimide film and use it for inkjet printing to create conductive circuits with 70-100 μm line widths. [19] They have also used surface energy patterning to print silver- and gold-electrodes for organic thin film transistors with a channel length of <25 μm. [20] Another method proposed by researchers is random patterning based on parallel vacuum ultraviolet (PVUV) technology, which successfully fabricated short-channel organic thin-film transistors (OTFTs) with widths down to 1 μm on PET substrates in large areas. [21] These approaches have enabled the fabrication of small feature sizes, even below the footprint of a single drop.

There are two main methods to generate heterogeneous wettability patterns on the substrate. One is to selectively bond hydrophobic molecules on the hydrophilic substrate surface via microcontact printing with a pre-patterned soft stamp,[22] which has the advantages of convenience, high speed, and excellent compatibility with a wide range of materials. However, this method faces deformation problems due to unbalanced pressure and swelling in organic solvent[23]. The second method is to transfer the hydrophobic surface to hydrophilic through chemical etching,[24] RF plasma discharge,[25] and UV irradiation.[26, 27] The first two methods require a patterned shadow mask to generate heterogeneous wettability patterns. However, it has difficulties reaching micrometer structures owing to the challenges in making shadow masks on the micrometer scale. By contrast, UV light irradiation provides a shortcut to creating ultrafine heterogeneous wetting patterns based on the light-induced surface energy conversion,[21, 28, 29] since photomasks can be used for this purpose.

Surface energy conversion based on the photolysis and change of surface molecular conformation under light illumination was recently reported in the literature,[16] which showed the advantages of efficiency, non-invasive, and most importantly, compatibility with a photomask to realize a high resolution. Recently, Rossegger *et al.*[30] reported a photon-sensitive NBE derivative, which can polymerize with a fluorinated resin under white light ($\lambda > 400$ nm) illumination and then decompose by a UV light illumination ($\lambda < 400$ nm). More interestingly, the polymer film obtained by white light illumination has a hydrophobic surface with a water contact angle (WCA) as large as 107°, whereas the UV-light illuminated film showed a hydrophilic surface with a WCA of 7°. Such a surface wettability transformation manipulated by light illumination enables the precision manufacturing of fine structures through the printing process.

In this work, We have created a cost-effective and efficient method to coat large areas with flexible and patterned designs. We achieved this by utilizing a light-sensitive NBE-acrylate resin to prepare a diverse wetting surface. This surface energy variation limits the spread of ink, allowing for a printing resolution of 5 μm. This breakthrough process differs from conventional methods and offers significant advantages.we using NBE derivative-fluorinated resin composite film as the surface wettability tunning material for printing electronics. The NBE-Fluorinated resin composite was successfully polymerized by with LED light, which showed a WCA of 107°. Following a light illumination with a UV light of 254 nm, the polymer film was transferred to hydrophilic.

By using a photomask, fine microstructure with a line-and-space (L/S) of 10/10 μm or 5/50 μm was successfully achieved. With that, we developed the present technique to fabricate short-channel organic thin-film transistors (OTFTs) in large-area arrays on a plastic substrate.

2. Result and discussion

2.1 Materials synthesis and photon-induced surface energy conversion

The (2-nitro-1,4-phenylene) bis (methylene) diacrylate (Acrylate-NBE) was synthesized from (2-nitro-1,4-phenylene) dimethanol, according to Rossegger's report.[30] The synthesis scheme is shown in Scheme S1 in supporting information and detailed synthesis procedure is described in experiment part. Figure S1 shows the NMR of the final compound, which is in good accordance with the literature results,[30] demonstrating the successful synthesis of the target compound Acrylate-NBE.

In detail, a precursor film of (2-nitro-1,4-phenylene)bis(methylene) diacrylate (acrylate-NBE), cross-linker pentaerythritol tetra(3-mercaptopropionate)(PETMP), Fluorolink MD®700, with photoinitiator bisacylphosphine oxides phenylbis (2,4,6-trimethylbenzoyl)-phosphine oxide (BAPO) were mixed(see Scheme S2 in supporting information for the chemical structures) in $CHCl_3$ and the solution was spin-coated on the precleaned glass substrate (step i, see experiment part for details). The obtained viscous precursor nano thin film was cured with a white LED lamp to yield a polymer surface (step ii in Figure 1a), which showed a hydrophobic nature (*vide infra*). The film was then exposed to 254 nm UV light using a shadow or photo mask (step iii). Photolysis of the polymer film under UV light illumination yielded hydrophilic regions and generated heterogeneous wettability patterns. After that, hydrophilic inks were bar coated on the surface (step iv), where the ink on the hydrophobic region will be pushed to the hydrophilic region and expended over the hydrophilic region (step v). The drying of the solvent will yield the desired patterns with the solute.

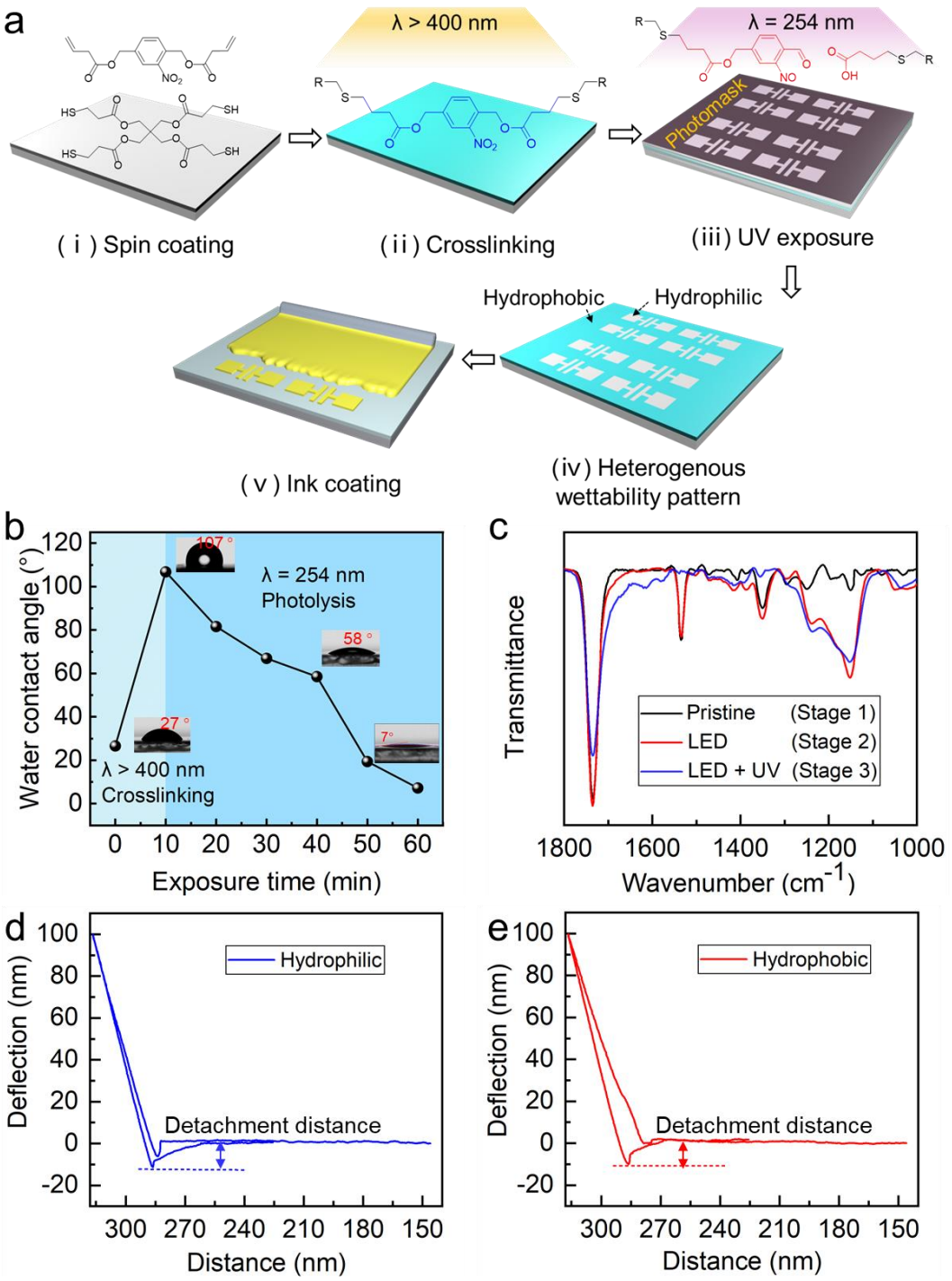

Figure 1. a). Process scheme for printing microscale electric circuit by UV-converted heterogeneous wettability surface; b) Evolution of the static water contact angle (WCA) on polymer surfaces under illumination, LED: white light curing with λ> 400 nm, 230 mW·cm^{-2}; UV light: λ= 254 nm, 15 mW·cm^{-2}; c) FTIR spectrum of the pristine and light illuminated polymer surface; d-e) Observation of light conversion by AFM force spectroscopy and force mapping.

The process for the preparation of printed fine electric circuits is shown in Figure 1a.

Figure 1b shows the static water contact angle (WCA) on the pristine and light-treated films. As seen here, the as-prepared pristine film showed a WCA of 27º, indicating a hydrophilic surface. After being curved with white LED light, the polymer film showed a large WCA of 107°, similar to that reported by Rossegger *et al*.,[30] demonstrating the formation of a cross-linked hydrophobic polymer surface. Upon UV light illumination (254 nm, 15 mW/cm^2), the WCA decreased significantly with the increase of illumination time, where a low WCA of 58° and 7° was measured for UV light illumination for 30 and 50 min, demonstrating the successful transfer the surface energy by UV light. FTIR spectra proved the conversion of the polymer surface via light illumination. Figure 1c shows the FTIR spectra of the films that after white light and UV illumination. As seen here, the absorption band at 1100-1300 cm^{-1} enhanced significantly after the white LED light curing, ascribing to the polymerization of acrylate with PETMP to form C-S-C bonds. Upon irradiation with UV light, the nitro groups are converted to nitroso moieties leading to a decrease of the two characteristic NO_2 absorption bands at 1537 cm^{-1} (asymmetric stretching) and 1348 cm^{-1} (symmetric stretching).[31, 32] In addition, a broadening of the C=O absorption band at 1735 cm^{-1} is observed, which is associated with the breakage of polar groups to produce carboxylic acids.[33]

In addition, we checked the surface adhesion force of the film. AFM tips are used to approach the film, allowed to dwell on the surface and then retracted from the surface. The force spectra of such approach and retraction are recorded as shown in Fig. 1d and 1e. As can be seen here, a large jump in the retraction trace of the force spectrum curve about the film is observed for the tip leaving the surface, which is a non-specific adhesion between the AFM tip and the film.[34] Where the distance from the dotted line to the baseline position is the distance of the tip's detachment, 10.03 nm in the hydrophilic region and 11.4 nm in the hydrophobic region. Based on the tip This difference indicates that the adhesion on the surface of the film changes before and after light exposure. Both the FTIR and AFM results clearly confirmed the photolysis of the cross-linked polymers after UV illumination.

2.2 Formation of patterned heterogeneous wetting surfaces via UV-light illumination

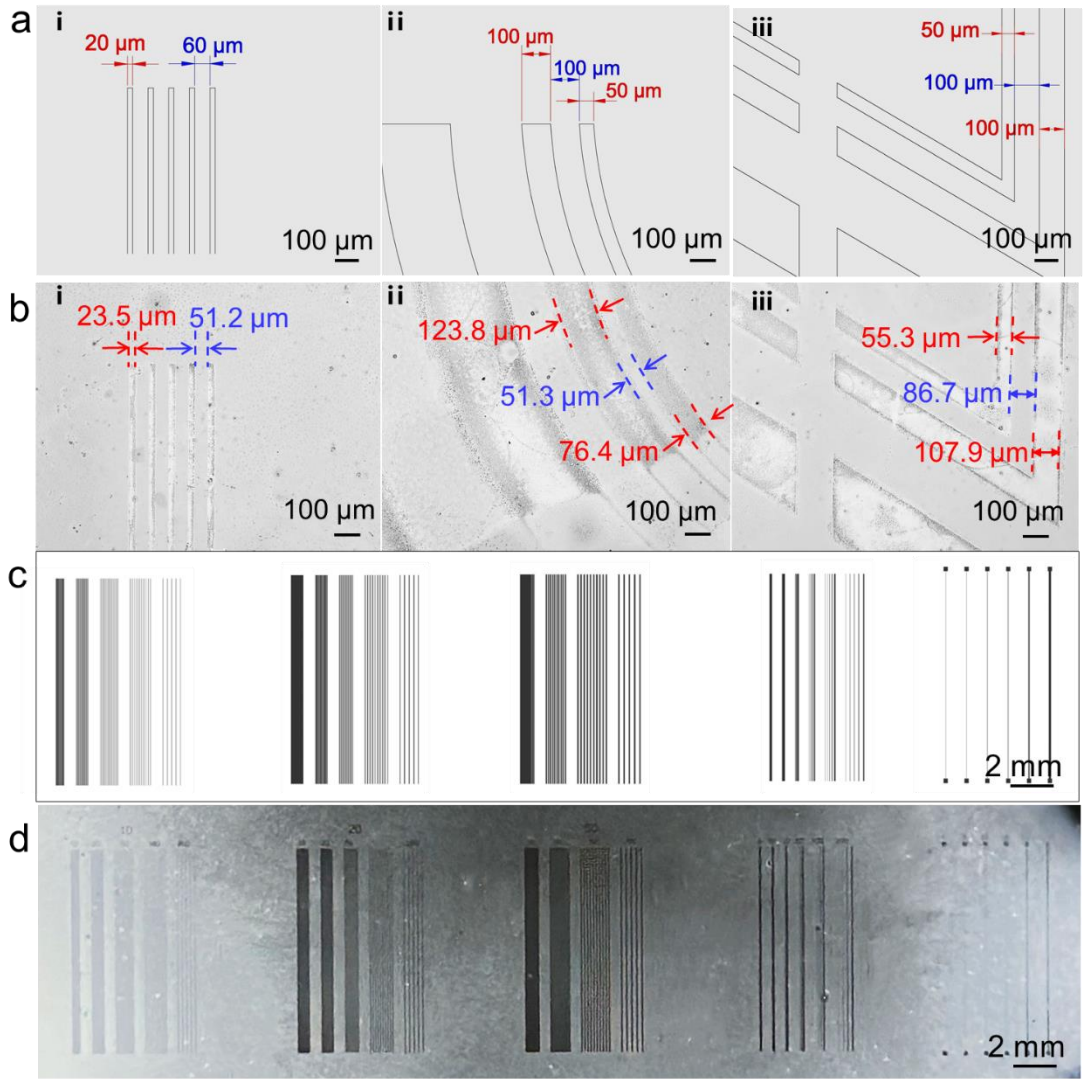

Figure 2. a) Pattern structure of the shadow mask; b) 3D laser confocal microscopy images of the polymer surface after UV exposure with shadow mask; c) Pattern parallel lines of the chromium-based photomask; d) Optical images of polymer surface after saturated with water vapor.

To confirm that this polymer surface energy conversion can generate heterogeneous wettability patterns for precision printing manufacture, we first checked the surface transformation under 254 nm UV light illumination covered with a patterned shadow mask. Figure 2a shows the designed shadow mask structure, and Figure 2b shows the 3D laser confocal microscopy images of the surface after UV light irradiation for 50 min, as described in Figure 1a, step iii. As is seen here, the designed patterns were successfully transferred from the shadow mask to the polymer surface. Both parallel lines with different line-width-to-space (L/S) and annular lines with a diamond or circle structure were obtained. However, compared to the mask setting of 20 and 60 μm for the line width and line space (Figure 2ai)., the obtained line width and line

spacing were measured to be 23.5 ± 0.5 and 51.2 ± 0.5 μm (Figure 2bi), demonstrating that light exposure expends the line width but compresses the line spacing. A similar phenomenon was also found in designed diamond and circle structures (ii and iii in Figures 2a and 2b). This can be ascribed to the divergent light source and unsatisfied contact between the mask and the polymer surface.

Owning to the resolution limitation of the shadow mask, the smallest line width is limited to 20 μm when using a shadow mask. To further test the resolution limit of this UV-assistant heterogenous wettability fabrication method, we use a chromium-based photomask for the same UV-exposure procedure. Figure 2c shows designed patterns with parallel lines of a small L/S of 5/50 and 10/10. We then checked the surface topology of the UV-exposed sample with 3D laser confocal microscope. However, the polymer surface exposed with a chromium photomask showed no design pattern after UV exposure (data not shown), indicating no noticeable surface topology changes upon UV light illumination. Although AFM measurement confirmed the change of surface adhesion force upon UV light illumination (*vide supra*), we could not get the patterned structure with AFM, which was ascribed to the inappropriate AFM tips. After being put on top of water vapor for a while, the designed patterns with a small L/S of 5/50 can be developed (Figure 2d). These results demonstrate the successful transformation of the local hydrophobic surface to hydrophilic surface upon UV exposure with a photomask.

2.3 Ink formulation and dewetting on the heterogenous surface

In general, the formation of fine structures on a heterogenous wettability surface includes the following three steps. First, the ink is deposited onto the entire surface to form a continuous wet film. The ink solution on the dewetting region will recede during the drying, while the ink is pinned locally on the wetting region and form liquid puddles. The final drying of the ink solution on the wetting region will leave desired patterned structure according to the mask (Step v in Figure 1a). Such an ink solution movement and drying process highly depends on the substrate's surface energy and the ink's rheology. We, therefore, carefully manipulated the ink formulation and checked the rheology of the conductive silver inks.

Water and diethylene glycol monomethyl ester (DGME) are the most commonly used organic solvents for dispersing silver nanoparticles. It is known that the rheological properties of the inks will affect the movement of ink droplets on the surface. We measured the viscosity of the silver nanoparticle inks with different solvent mixtures.

Figure 3a shows the viscosity of the ink at different shear rates. As seen here, all these inks are typical shear-thinning fluids whose viscosity decreases gradually with the increase of the shear rate. This indicates that a certain shear force is required to promote the fluidity of the ink during the coating process. The viscosity of these silver inks was measured to be 15-18 mPa·s, and no significant influence of the solvent mixture on the viscosity was found.

We then check the contact angle of water, DGME and the mixture solvent of water:DGME on the hydrophobic and hydrophilic surfaces, respectively. Figure 3b shows the variation of contact angles that content of the mixture solvent. Although a high WCA of 107° was measured for the water droplet in the hydrophobic region, the contact angle of DGME droplet on the pristine polymer surface is only 48°. On the other hand, the contact angle of DGME on the UV-treated region was measured to be 15°, which is similar to that of water on the hydrophilic surface, demonstrating a good wettability of DGME on the hydrophilic region as well. The mixture solvent of water:DGME (1:1, v/v) showed a reduced contact angle of 74° on the hydrophobic region, which is further reduced to 63°, 64° and 59° for the 1:2, 1:3 and 1:4 mixture solvent, whereas the contact angle of the mixture solvent on the hydrophilic region is lower than 15° for all blend ratios. Thus, the contact angle difference for all these mixed solvents on the hydrophobic and hydrophilic regions is higher than 50°, which ensures a sufficient driving force for the surface dewetting process.[16]

After carefully measuring the contact angle of water and CH_2I_2 on the hydrophobic and hydrophilic surfaces (Figure S2 in supporting information). We obtained the wetting envelope by using the calculations from the WORK model. [35] The wetting envelope of the hydrophobic and the hydrophilic surfaces are shown in Figures 3c and 3d. As seen here, water showed a dewetting nature (with a large contact angle of over 100°) on the hydrophobic surface, whereas it showed a wetting feature (with a low contact angle of less than 10°) on the hydrophilic surface. On contrast, DGME shows good wetting on both hydrophobic (with a contact angle of less than 60°) and hydrophilic surfaces (with a contact angle of less than 20°). The water:GDME mixture solvents were also measured. An increased dewetting feature on the hydrophobic surface was found with increased water content while keeping a good wetting nature on the hydrophilic surface. This will enable a suitable solvent for separating the droplets during printing.

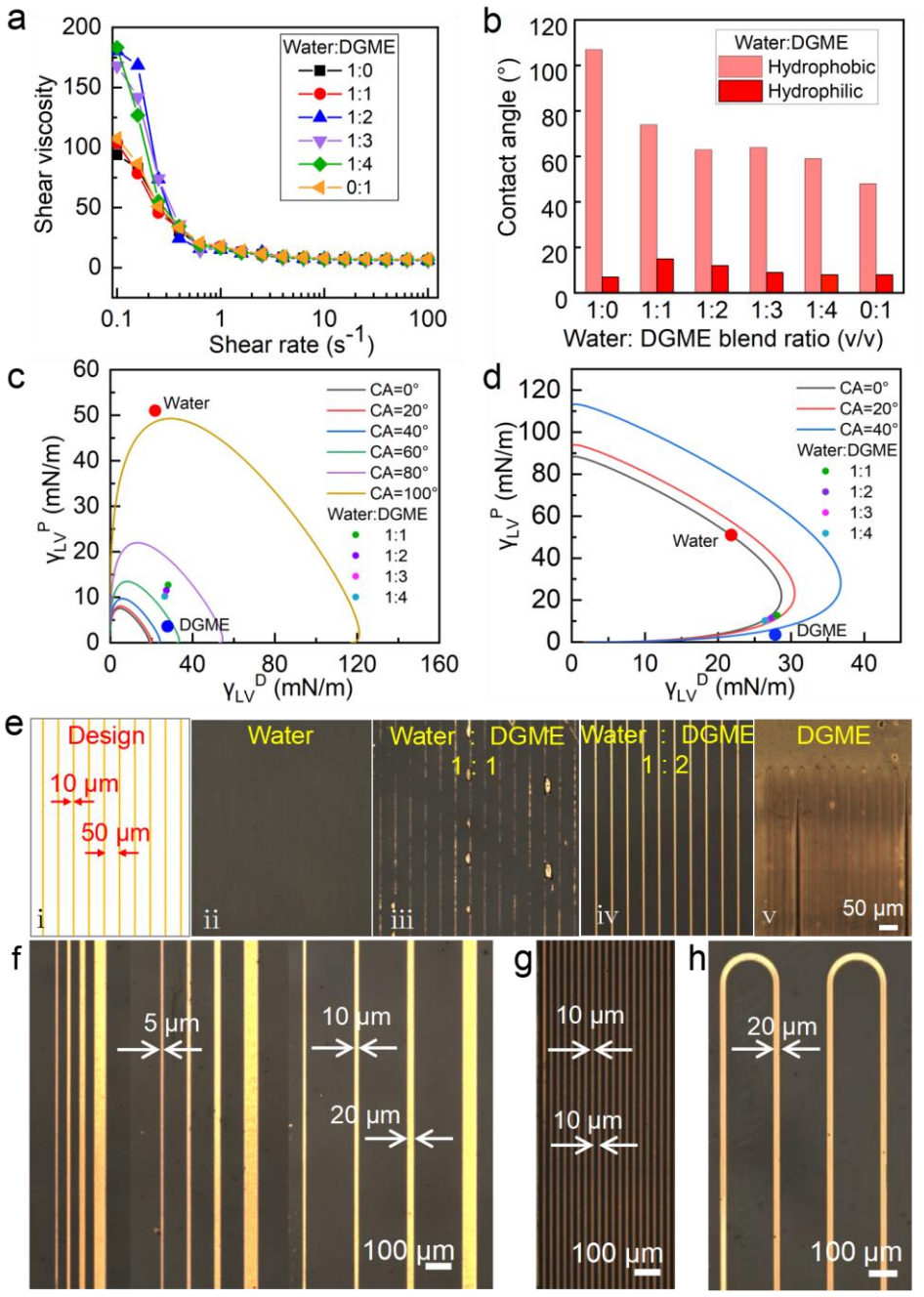

Figure 3. a) Viscosity of the silver ink formulations as a function of shear rate; b) Contact angles of the water:diethylene glycol monomethyl ester (DGME) on the hydrophobic (the pristine) and hydrophilic (UV-treated) surface, the blend ratio is in volume; c) Wetting envelope at the hydrophobic surface; d) Wetting envelope at the hydrophilic surface; e) Surface morphology of the dried film coated from different silver inks, the designed pattern of the photomask (with L/S of 10/50 μm) is shown on the left; f) Sample of the fine circuits with line width of 5, 10, 20, 50 μm and a pitch of 50, 100 and 200 μm, respectively; g) Sample of the fine circuits with line width of with L/S of 10/50 μm; h) Complex electronic circuits with a line width of 20 μm.

We then test the formation of fine electric circuits on the heterogenous wettability patterns surface for different inks according to the process listed in Figure 1a. Figure 3e shows the results. Interestingly, although a high contact difference was measured for water, no silver trace was left on the patterned surface (Figure 3e-ii), indicating surface tension is not the only parameter determining the dewetting process. In contrast, the DGME-based ink showed an almost continuous silver film on the surface (Figure 3e-v), indicating insufficient driving force for separating the ink. The ink based on water and DGME 1:2 showed clear parallel silver lines with L/S of 10/50 (Figure 3e-iv), which is in good accordance with the designed pattern (Figure 3e-i). The successful preparation of silver lines could be due to the solid surface's balanced surface tension and surface energy.

Using the optimized ink formulation, we then verified the preparation of fine patterns. Figure 3f shows the parallel lines with 5/10/20/50 μm line widths and a spacing of 50/100/200 μm, respectively. As seen here, fine lines with line width as low as 5 μm were successfully achieved when the line space is higher than 50 μm. Although further reducing the line spacing to 20 μm led to the fusion of 5 μm lines (Figure S4 in supporting information), parallel line patterns with a L/S of 10/10 μm were successfully prepared（Figure 3g）, which is much better than the traditional printing process. In addition to the parallel lines, arcs with a line width and radius of 20 and 75 μm were also successfully prepared (Figure 3h), demonstrating the potential application in arbitrary patterns.

2.4 Fully solution-processed flexible TFTs based on printed silver electrodes

We then prepared electrodes with different channel widths for thin film transistors. Figure 4b shows the optical microscope images of the printed electrodes on glass with channel widths of 15-80 μm. As seen here, the obtained channel width is slightly lower than the designed one, which could be due to the light scattering effect and not ideal contact between the photomask and the polymer surface. Figure S5 in supporting information shows the microscope images of these electrode arrays on glass. Although the printing process was not fully optimized, only few defects were measured for an effective area of 4 cm^2. SEM measurement confirmed a compact and continuous silver film for the printed silver electrode (Figure 4c). The same method successfully prepared electrode arrays on a flexible PI substrate with an overall size of 1.5 × 2.5 cm^2. It is

worth noting that thermal annealing was performed on the printed electrode to enhance the conductivity. Figure 4e shows the I-V characteristics of the electrodes after thermal annealing at different positions. According to Figure S6, the electrode's conductivity was measured at a distance of around 400 μm and showed a high current of over 0.2 A at a voltage of 1 V. This indicates that the conductivity is over 10^5 $S \cdot m^{-1}$. In contrast, a low current of less than 10^{-12} A was measured for two electrodes over a broken channel, indicating a clean channel was prepared by this method. It worth noting that surface imhomogenity was measured for the printed electrode, which could be due to non-optimized substrate surface and ink formulation that leads to coffee-ring effect during the drying of the film. This phenomenous was also reported by Li et al. and can be improved by substrate surface modification.[28] Nevertheless, the prepared electrodes meet the requirements of TFT preparation.

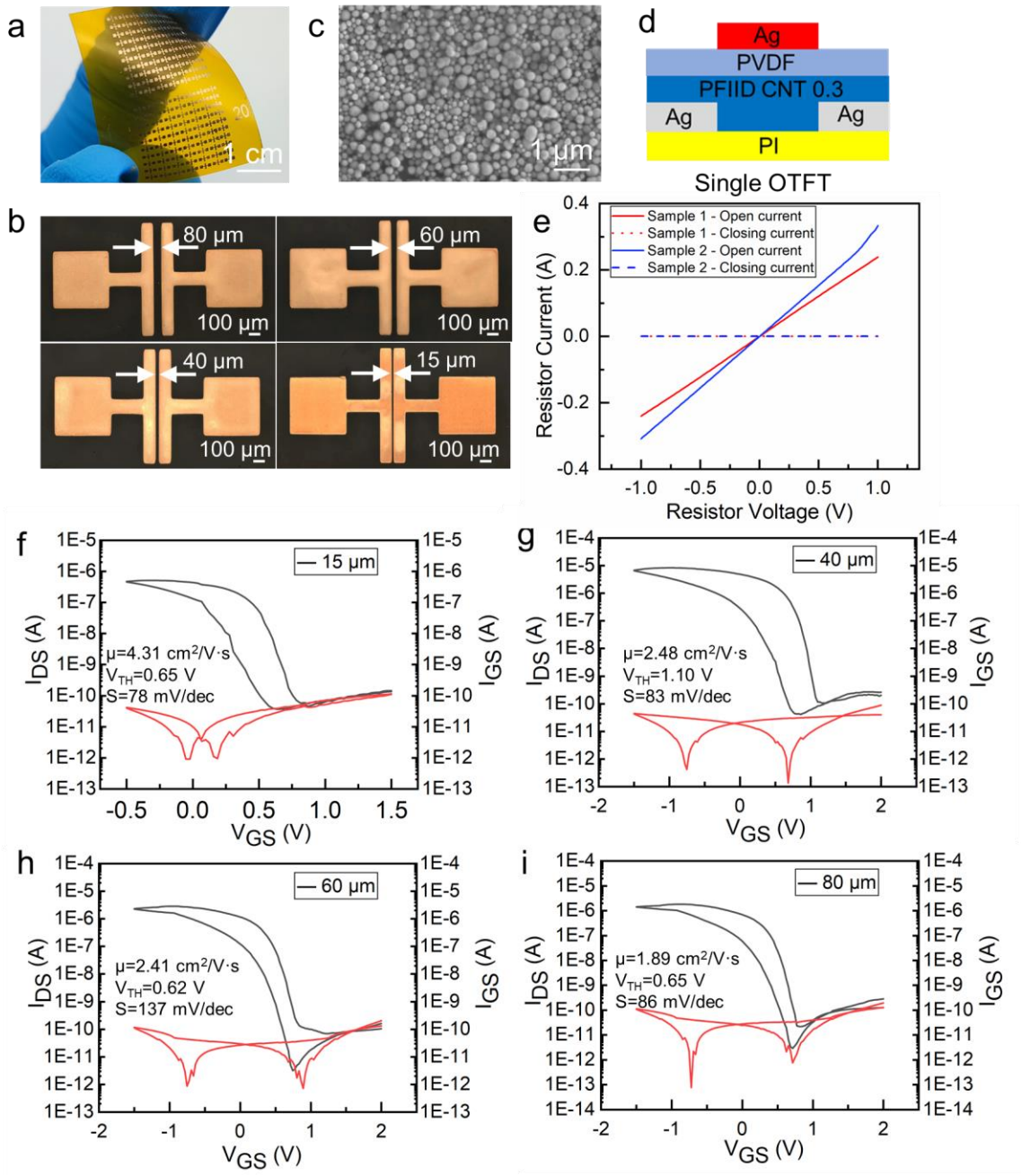

Figure 4. a). Flexible OTFT arrays on polyimide substrate with a total size of 1.5 × 2.5 cm^2; b). Optical microscopes of the prepared bottom electrodes with different channel widths; c). SEM image of the prepared silver electrode; d). Structure of carbon nanotube (CNT)-based OTFT; e). measured I-V curves on the electrode with a space of 400 μm; f-i) Output and transfer I-V curves of the TFT with a channel width of 15 (f), 40 (g), 60 (h), and 80 (i) μm.

Finally, flexible thin film transistors based on PI were prepared by full solution processes (Figure S7 in supporting information). Figure 4d shows the structure of the bottom-contact-top-gate TFT, where the bottom silver electrodes were fabricated by the method developed described above. In detail, the flexible electrodes were prepared

according to the method described above, and carbon nanotubes were deposited onto the channel by aerosol jet printing. The PVDF layer and the gate electrodes are prepared by inkjet printing. Figure 4f-i shows the output and transfer curves of the transistors with different channel lengths. The characteristic performance data, including current switch ratio (I_{ON}/I_{OFF}), mobility (μ), threshold voltage (V_{TH}), and subthreshold swing (SS). As seen here, all these transistors showed high I_{ON}/I_{OFF} ratios of 10^4 and high charge carrier mobility (μ) of 1.89-4.31 $cm^2\ s^{-1}\ V^{-1}$. In addition, the subthreshold swing (SS) of the devices is less than 137 mV/dec indicating a high modulation efficiency of the devices. The device threshold voltages of these devices were measured to be 0.62-1.10 V, indicating a depletion mode of these transistors, which could be due to the polymer residue of printing ink that exacerbates carrier surface scattering and trap state generation. Nevertheless, fabricating fully functional OFETs on such surface energy patterned substrates shows that the additional pre-structuring steps do not affect the device's performance.

Conclusion

In this work, we report the use of NBE derivative-fluorinated resin composite film as the surface wettability tunning materials for printing electronics. The ink can be spontaneously patterned by utilizing the difference in surface energy. This process is advantageous because it requires simple equipment, allows for large flexible areas and high resolution, and enables patterned printing through scratching. The NBE-Fluorinated resin composite was successfully polymerized by with LED light, which showed a water contact angle (WCA) of 107°. Following a light illumination with a UV light of 254 nm, the polymer film was transferred to hydrophilic with a low of 7°. A high WCAB contrast of over 50° was measured for the hydrophobic and hydrophilic area, which makes the heterogeneous wetting surface suitable for precision printing manufacturing find circuits. Through ink formulation, fine microstructures with a L/S of 10/10 μm or 5/50 μm were successfully achieved. Furthermore, we developed the present technique to fabricate short-channel organic thin-film transistors (OTFTs) in large-area arrays on a plastic substrate. Additionally, we could show that the additional pre-structuring steps have no negative influence on the device's performance.

Experimental

Materials

The photoinitiator phenyl bis(2,4,6-trimethylbenzoyl)-phosphine oxide (BAPO), Pentaerythritol tetra(3-mercaptopropionate) (PETMP), 2-Nitro-p-xylylene Glycol were from TCL-SCT. Fluorolink MD®700 was supplied by Foshan Zhaojing Environmental Protection Technology Co. Ltd. Isobornyl acrylate was obtained from J&K Scientific. Acryloyl Chloride was provided by Adamas-beta. Bruno Bock Thiochemicals (Germany). All chemicals were used without further purification. (2-nitro-1,4-phenylene) bis (methylene) diacrylate（acrylate-NBE）was synthesized as previously reported.[30]

Synthesis (2-Nitro-1,4-phenylene) bis (methylene) diacrylate

Acryloyl chloride (6.7 mL; 82 mmol) was mixed with a solution of (2-nitro-1,4-phenylene) dimethanol (5 g; 27 mmol) in 50 mL dry THF. Triethylamine (7.7 mL, 55 mmol) was dissolved in 50 mL dry THF and added dropwise to the reaction mixture. The reaction mixture was stirred overnight at room tempera-ture and the progress was monitored by TLC. After evaporation of the solvent, the crude oil was dissolved in dichloromethane and extracted with water and saturated Na_2CO_3 solution. The combined organic layers were dried over $MgSO_4$ and the solvent was removed by rotary evaporation. Chromatography on silica gel (cyclohexane:ethyl acetate = 2:1) resulted in 3.2 g white crystals of acrylate-NBE (40% theoretical yield).

^{1}H NMR (δ, 400 MHz, 25 °C, $CDCl_3$): δ 8.16-8.15 (d, 1H), 7.69-7.67 (dd, J=8.0, 1.6Hz, 1H), 7.64-7.62 (d, 1H), 6.54-6.48 (q, 2H), 6.27-6.17 (m, 2H), 5.97-5.92 (m, 2H), 5.63 (s, 2H), 5.29 (s, 2H).(Figure S1, Supporting Information)

Preparation of patterned hydrophilic and hydrophobic substrate

Resin formulations were produced by mixing acrylate-NBE and isobornyl acrylate in an equimolar ratio of 37.5 mol% with 1 wt% of the fluorinated methacrylate (Fluorolink MD®700). The thiol content was 25 mol%. 2.5 wt% BAPO was used as a photoinitiator. Dissolved the resin components in chloroform and stirred in an ultrasonic bath for 10 minutes. To prepare the sample, the solution was spin coated on a clean glass substrate. Irradiation with visible light (HSPY-60-05 LED curing lamp, 230mW/cm^2, 420 nm) to generate a hydrophobic film. Then the cured samples were exposed to UV light

(ZB254-150UV; 15mW/cm^2; 254 nm) to selectively irradiate the polymer film through a contact photomask for 1200 s in air.

Spontaneous patterning of complex electronic circuits

This study utilized Ag ink (SicrysTMI40DM-106) for patterning conductive patterns, and Ag nanoparticle ink was deposited on the entire hydrophilic and hydrophobic patterned substrate through a common scratch coating process to form conductive patterns spontaneously. The scraper moved at a speed of 1mm/s. After the ink self-assembly, the formed complex electronic circuits were dried directly under ambient conditions and then sintered at 300 °C for 30 minutes.

Preparation of transistor devices by solution method

Preparation of active layer: the separated and purified semiconductor P2 ink forms aerosol fog under the action of ultrasound, and the channel shape is introduced into the program. By adjusting the printing parameters, a semiconductor film with uniform thickness and complete patterning is obtained. After annealing at 120 ℃ for 3 min, it is cooled at room temperature for 3 min, and the active layer channel area is flushed with toluene solution to remove the excess polymer and impurities in the carbon nanotube network and enhance the conductivity of the semiconducting single-walled carbon nanotube network. After that, the single-walled carbon nanotube network was efficiently immobilized by annealing at 120 ℃ for 30 min.

Preparation method of grid electrode: Inject the advanced nano products (DGP 45HTG) into the inkjet cartridge with a 1mL syringe and store it in a refrigerator at 2 ℃. The sample is fixed on the stand of the inkjet printer (Dimatix USA, DMP-2831). After installing the ink cartridge, the print waveform of silver nanoparticle ink is loaded into the program, the print parameters are adjusted, and the print temperature of 50 ℃ is maintained to prevent ink droplets from diffusing on the substrate. Adjust the size and spacing of printing ink drops to adapt them to glass and PI film substrates. Design the shape of the grid electrode, import it into the program, and print the point-to-point position accurately. After the inkjet printing is completed, the printed graphics need to be placed on a 150 ℃ hot table for high-temperature annealing for 30 minutes to remove the solvent in the silver nanoparticle ink and complete the sintering of silver

nanoparticle to enhance the conductivity of the pattern.

Acknowledgments:

The authors would like to acknowledge the financial support from Guangdong Basic and Applied Basic Research Foundation (2020B1515120059), and the Postdoctoral Programm of Guangdong Institute of Semiconductor Micro-Nano Manufacturing Technology (2022BA09000).

References

[1] Buga C S; Viana J C **2022** The role of printed electronics and related technologies in the development of smart connected products *Flexible Printed Electron.* 4 043001

[2] Beedasy V; Smith P J **2020** Printed Electronics as Prepared by Inkjet Printing *Materials.* 3 704

[3] McDowell C; Bazan G C **2017** Organic solar cells processed from green solvents *Curr. Opin. Green Sustainable Chem.* 49-54

[4] Li W B; Zhang C; Lan D; Ji W J; Wang Y R **2022** Solution Printing of Electronics and Sensors: Applicability and Application in Space *Adv. Eng. Mater.* 9 2200173

[5] Labiano I I; Alomainy A **2021** Flexible inkjet-printed graphene antenna on Kapton *Flexible Printed Electron.* 2 025010

[6] Ramon E; Sowade E; Martinez-Domingo C; Mitra K Y; Alcalde A; Baumann R R; Carrabina J **2021** Large-scale fabrication of all-inkjet-printed resistors and WORM memories on flexible polymer films with high yield and stability *Flexible Printed Electron.* 1 015003

[7] Boda U; Strandberg J; Eriksson J; Liu X; Beni V; Tybrandt K **2023** Screen-Printed Corrosion-Resistant and Long-Term Stable Stretchable Electronics Based on AgAu Microflake Conductors *ACS Appl Mater Interfaces.* 9 12372-12382

[8] Lee Y; Han Y J; Cho K Y; Cho K H; Jeong Y C **2021** Large-Scale and High-Resolution Patterning Based on the Intense Pulsed Light Transfer of Inkjet-Printed Light-Emitting Materials *Macromol Res.* 2 172-177

[9] Wang H; Zhang Y; Liu Y; Chen Z; Li Y; Li X; Xu X **2023** High-efficiency and high-resolution patterned quantum dot light emitting diodes by electrohydrodynamic printing *Nanoscale Adv.* 4 1183-1189

[10] Go M; Qi X; Matteini P; Hwang B; Lim S **2021** High resolution screen-printing of carbon black/carbon nanotube composite for stretchable and wearable strain sensor with controllable sensitivity *Sensor Actuat A-phys.* 113098

[11] Secor E B; Lim S; Zhang H; Frisbie C D; Francis L F; Hersam M C **2014** Gravure Printing of Graphene for Large-Area Flexible Electronics *Adv. Mater.* 26 4533-4538

[12] Fukuda K; Someya T **2017** Recent Progress in the Development of Printed Thin-Film Transistors and Circuits with High-Resolution Printing Technology *Adv. Mater.* 25

[13] Hatt T; Bartsch J; Davis V; Richter A; Kluska S; Glunz S W; Glatthaar M; Fischer A **2021** Hydrophobic AlO(x) Surfaces by Adsorption of a SAM on Large Areas for Application in Solar Cell Metallization Patterning *ACS Appl Mater Interfaces.* 4 5803-5813

[14] Tian D; Song Y; Jiang L **2013** Patterning of controllable surface wettability for printing techniques *Chem. Soc. Rev.* 12 5184-209

[15] Sun J Z; Guo Y Z; Cui B; Chu F Q; Li H Z; Li Y; He M; Ding D; Liu R P; Li L H; Song Y L **2018** Inkjet printing bendable circuits based on an oil-water interface reaction *Appl. Surf. Sci.* 391-397

[16] Rossegger E; Hennen D; Griesser T; Roppolo I; Schlogl S **2019** Directed motion of water droplets on multi-gradient photopolymer surfaces *Polymer Chemistry.* 15 1882-1893

[17] Vafaei S; Tuck C; Ashcroft I; Wildman R **2016** Surface microstructuring to modify wettability for 3D printing of nano-filled inks *Chem. Eng. Res. Des.* 414-420

[18] Kooij E S; Jansen H P; Bliznyuk O; Poelsema B; Zandvliet H J W **2012** Directional wetting on chemically patterned substrates *Colloid Surface A.* 328-333

[19] Kim C; Nogi M; Suganuma K; Yamato Y **2012** Inkjet-printed lines with well-defined morphologies and low electrical resistance on repellent pore-structured polyimide films *ACS Appl Mater Interfaces.* 4 2168-2173

[20] Schlisske S; Raths S; Ruiz-Preciado L A; Lemmer U; Exner K; Hernandez-Sosa G **2021** Surface energy patterning for ink-independent process optimization of inkjet-printed electronics *Flexible Printed Electron.* 1 015002

[21] Liu X; Kanehara M; Liu C; Sakamoto K; Yasuda T; Takeya J; Minari T **2016** High-Resolution Electronics: Spontaneous Patterning of High-Resolution Electronics via Parallel Vacuum Ultraviolet *Adv. Mater.* 31 6768-6768

[22] Gebremichael Z T; Alam S; Cefarin N; Pozzato A; Yohannes T; Schubert U S; Hoppe H; Tormen M **2022** Controlling Metal Halide Perovskite Crystal Growth via Microcontact Printed Hydrophobic-Hydrophilic Templates *Crystal Research Technology.* 2 2100121

[23] Perl A; Reinhoudt D N; Huskens J **2009** Microcontact Printing: Limitations and Achievements *Adv. Mater.* 22 2257-2268

[24] Wang J Q; Yan Y D; Geng Y Q **2023** Fabrication of Chiral Nanostructures through Vibration-Assisted Scratching Combined with Wet Etching for Surface-Enhanced Raman Scattering Substrates *ACS Appl. Nano Mater.* 7 5860-5870

[25] Hong Y; You X Q; Zeng Y; Chen Y M; Huang Y Z; He W; Wang S X; Wang C; Zhou G Y; Su X H; Zhan W H **2019** Air-plasma surface modification of epoxy resin substrate to improve electroless copper plating of printed circuit board *Vacuum.* 108967

[26] Jin J; Ren H H; Liu Z Y **2020** Large-Area Patterning of Oil-Based Inks on Superhydrophobic TiO2 Nanotubular Layers by Photocatalytic Wettability Conversion *Catalysts.* 10 1203

[27] Ren P; Liu Y X; Song R Q; O'Connor B; Dong J Y; Zhu Y **2021** Achieving High-Resolution Electrohydrodynamic Printing of Nanowires on Elastomeric Substrates through Surface Modification *ACS Appl. Electron. Mater.* 1 192-202

[28] Li L; Li W; Sun Q; Liu X; Jiu J; Tenjimbayashi M; Kanehara M; Nakayama T; Minari T **2021** Dual Surface Architectonics for Directed Self-Assembly of Ultrahigh-Resolution Electronics *Small.* 26 e2101754

[29] Wang S T; Song Y L; Jiang L **2007** Photoresponsive surfaces with controllable wettability *J. Photochem. Photobiol. C Photochem.* 1 18-29

[30] Rossegger E; Nees D; Turisser S; Radl S; Griesser T; Schlogl S **2020** Photo-switching of surface wettability on micropatterned photopolymers for fast transport of water droplets over a long-distance *Polymer Chemistry.* 18 3125-3135

[31] Radl S V; Schipfer C; Kaiser S; Moser A; Kaynak B; Kern W; Schlogl S **2017** Photo-responsive thiol-ene networks for the design of switchable polymer patterns *Polymer Chemistry.* 9 1562-1572

[32] Giebler M; Alabiso W; Wieser V; Radl S; Schlogl S **2021** Photopatternable and Rewritable Epoxy-Anhydride Vitrimers *Macromol. Rapid Commun.* 2 e2000466

[33] Yan H X; He Y F; Yao L R; Wang X X; Zhang X Y; Zhang Y H; Han D X; Li C S; Sun L G; Zhang J Q **2022** Thermo-crosslinking assisted preparation of thiol-acrylate main-chain liquid-crystalline elastomers *J. Polym. Res.* 11 450

[34] Huang X; Li X; Wang Q; Dai J; Hou J; Chen L **2013** Single-molecule level binding force between collagen and collagen binding domain-growth factor conjugates *Biomaterials.* 26 6139-6146

[35] Fowkes F M J I; Chemistry E **1964** Attractive forces at interfaces 12 40-52

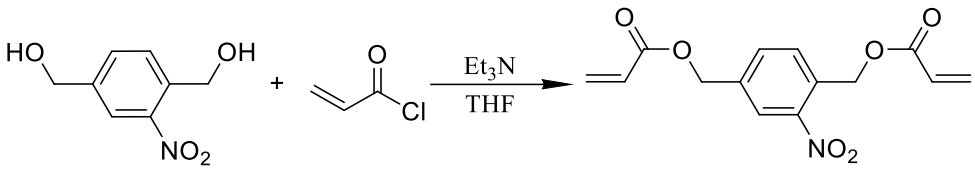

Scheme S1. Synthesis of acrylate-NBE

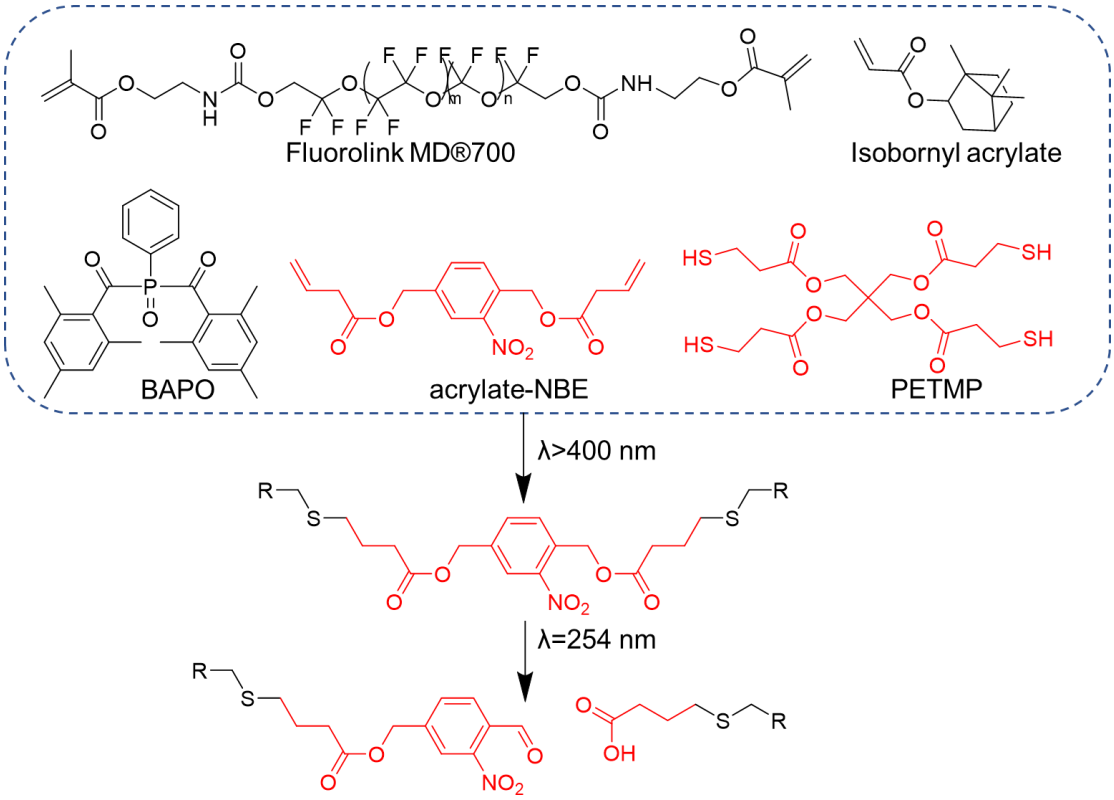

Scheme S2. Functional acrylates, fluorinated methacrylate, photoinitiator (BAPO) and multi-functional thiol (PETMP) used for the preparation of micropatterned acrylate and thiol-acrylate photopolymers with surface energy differences.

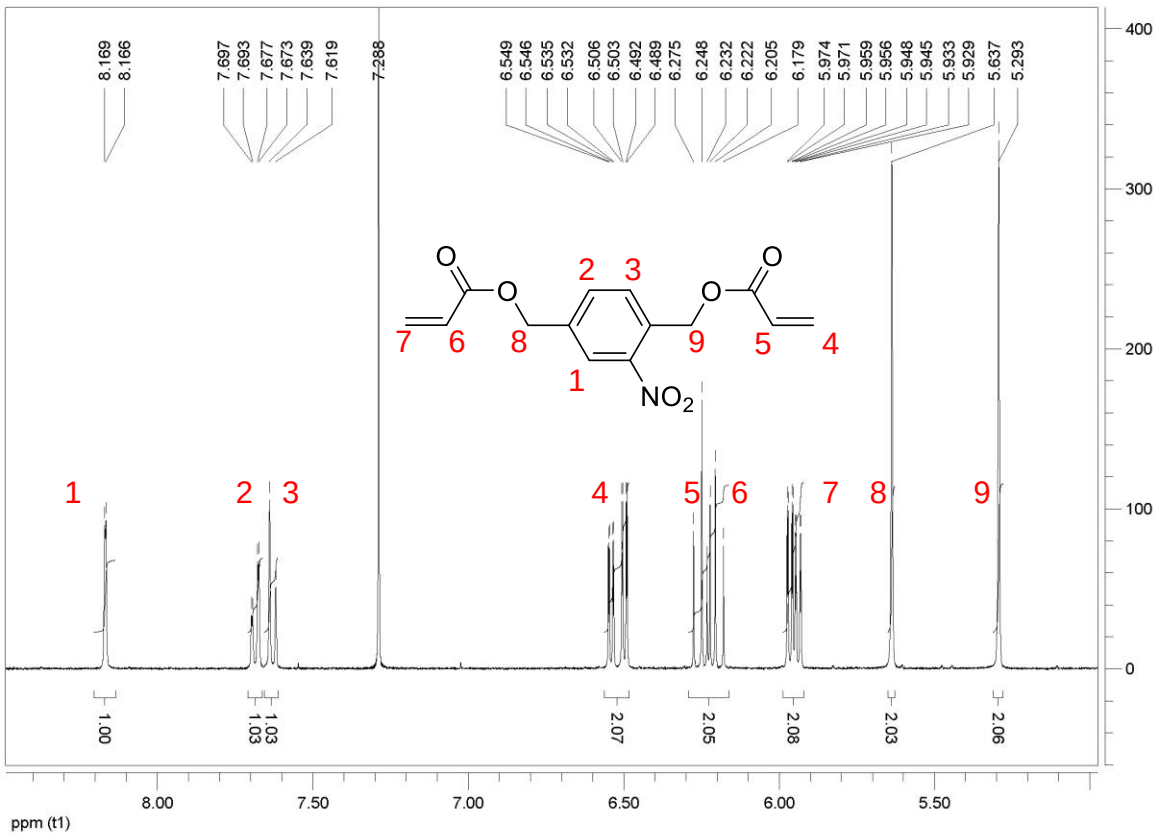

Figure S1. ^{1}H-NMR spectrum of acrylate-NBE

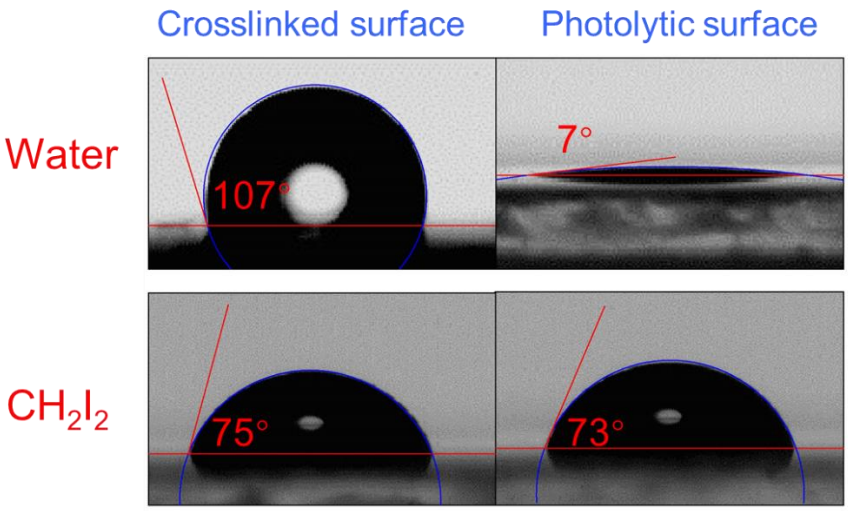

Figure S2. Static droplet contact angle

In this analysis, we use the Owens, Wendt, Rabel and Kaelble (OWRK) model.

The Owens-Wendt-Rabel-Kaelble (OWRK) Model

A solid surface's surface free energy (SFE) can tell you a lot about how different liquids will interact with said surface. Liquid surface tension, solid SFE, and a liquid droplet's contact angle on the surface are all related. The Owens, Wendt, Rabel, and

Kaelble (OWRK) model helps us visualize these relationships and can help us better understand our system and choose materials.

In these analyses, where the liquid surface tension, γ_{LV}, is a sum of a dispersive component (γ_{LV}^{D} e.g. London dispersion forces) and polar component (γ_{LV}^{P}, e.g. hydrogen bonding) such that $\gamma_{LV} = \gamma_{LV}^{D} + \gamma_{LV}^{P}$. Likewise, the solid SFE, γ_{SV}, is a sum of dispersive and polar components such that $\gamma_{SV} = \gamma_{SV}^{D} + \gamma_{SV}^{P}$. Then the relationship between liquid surface tension, solid SFE, and the contact angle between the liquid and the solid is described by the OWRK equation:

$$\gamma_{LV}(1 + \cos\theta) = 2\left[(\gamma_{SV}^{D}\gamma_{LV}^{D})^{\frac{1}{2}} + (\gamma_{SV}^{P}\gamma_{LV}^{P})^{\frac{1}{2}}\right]$$

Where θ is the contact angle between the liquid and the solid. Some critical assumptions are made in the OWRK model: the liquid is pure, the solid is smooth and chemically homogenous, and there are no chemical reactions between the liquid and the solid. No natural system will completely satisfy all of these assumptions, but the OWRK model is a powerful model widely used in industry and academia to guide material selection.

According to the two-component model, the interfacial tension depends on whether polar and dispersed parts can form interactions with corresponding parts of the adjacent phase. For example, the interfacial tension concerning water as the polar liquid is more minor when the solid is also polar. If, on the other hand, the polar part of the solid is small, then the square root term (σpl·σps)1/2 assumes a low value. The polar interactions only contribute to reducing the interfacial tension; this corresponds to poor wetting and a high contact angle.

The following diagram symbolizes the different interactions using hands - only "matching" hands can link.

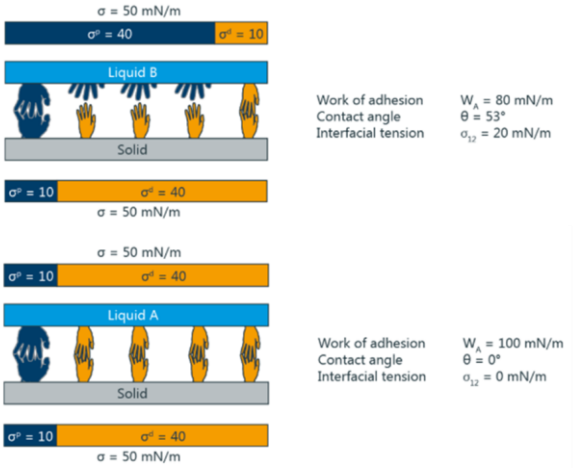

Schematic representation of the two-component phase contact model

Wetting Envelope

The relationship between liquid surface tension, solid SFE, and the contact angle of a liquid droplet can be better understood through wetting envelopes. These diagrams are beneficial in understanding how changes in polar and dispersive components of liquid surface tension will affect the contact angle.

Wetting envelopes help to visualize two essential concepts related to how surface tension affects contact angles. Firstly, when the polar and dispersive ratios of the liquid surface tension match those of the solid SFE, the contact angle will be minimized for a given γLV. Secondly, if γLV is low enough, the polar and dispersive ratios may not have much of an impact. The relationship between liquid surface tension, solid SFE, and the contact angle of a liquid droplet can be better understood through wetting envelopes. These diagrams are beneficial in understanding how changes in polar and dispersive components of liquid surface tension will affect the contact angle.

After carefully measuring the contact angle of water and CH_2I_2 on the hydrophobic and hydrophilic surfaces, substitute known parameters for the polar and dispersive forces of water and CH_2I_2. Eventually, polar and dispersion forces can be obtained for hydrophobic and hydrophilic solid surfaces. The surface energy is then calculated according to the OWRK equation by taking CA = 0°~100° respectively and assigning different scales of polar forces from 0 to 1. The corresponding values of the dispersion forces will also be obtained. From the data we get the wetting envelope.

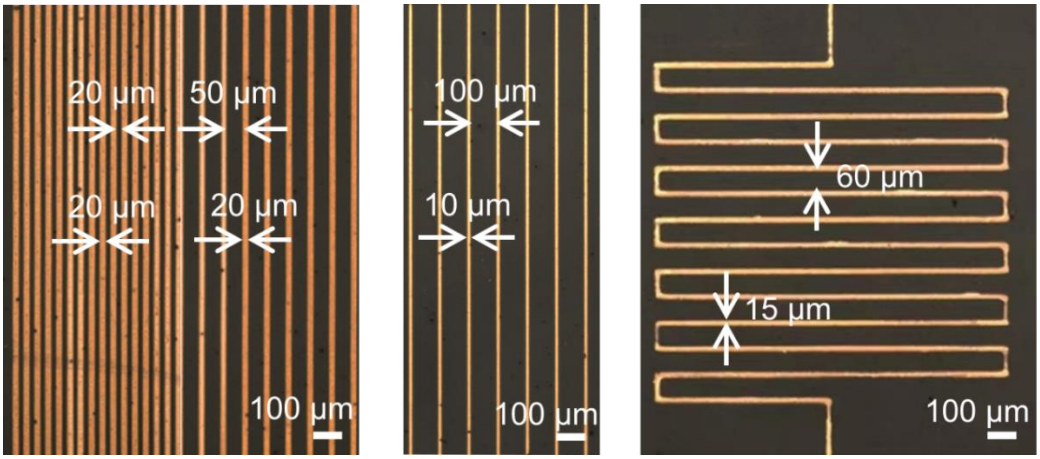

Figure S3. Print feasibility of complex circuits

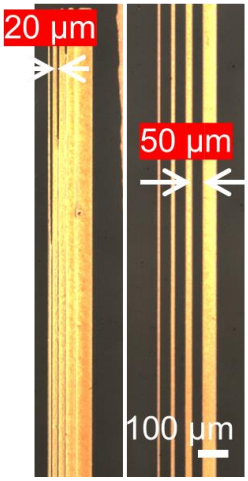

Figure S4. Print feasibility of complex circuits

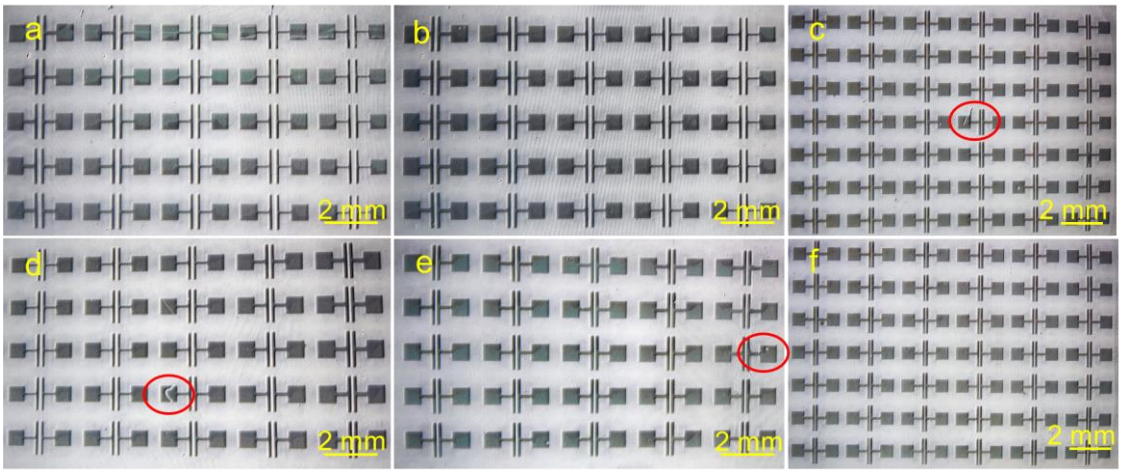

Figure S5. Large area transistor electrode arrays with different channel widths

、

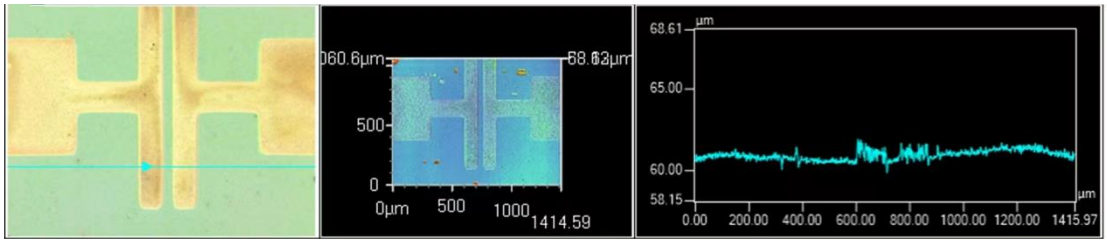

Figure S6. Thickness by 3D laser confocal microscopy

Electrical conductivity

Electrical conductivity σ is the reciprocal of resistivity. It is 1/ρ, measured in Siemens per metre (S/m).

$$\sigma = \frac{L}{R \cdot A}$$

Using the *I-V* curve displayed in Figure 4e, we have determined that R=3.81 Ω. Figure S6 provides additional information- the electrode thickness is 0.4 μm, the electrode single edge length measures 0.5 mm, and the cross-sectional area is $A = 2 \times 10^{-10}\ m^2$. The test needle is situated at the electrode's edge, resulting in an approximate distance of 0.4 μm. After plugging in these values, we arrived at a conductivity value of $5.2\times10^5\ S\cdot m^{-1}$.

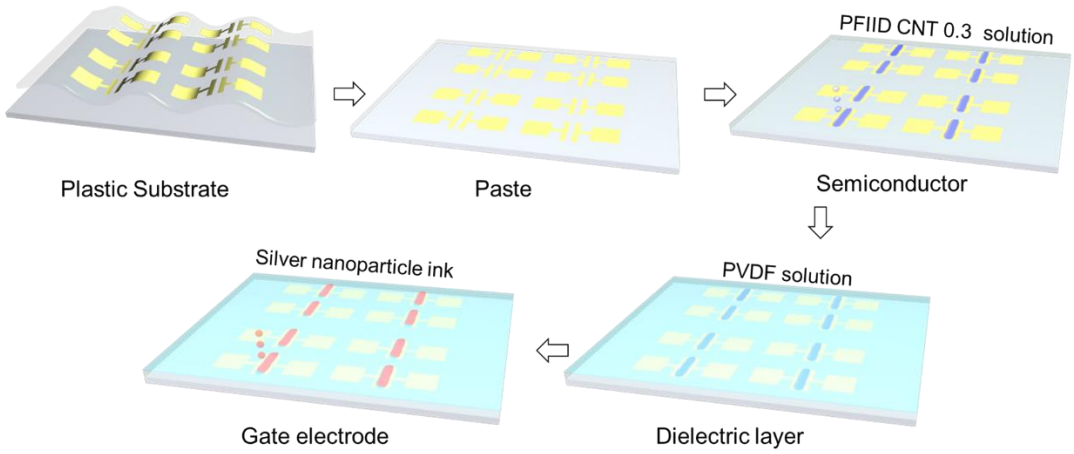

Figure S7. Print feasibility of complex circuits